Aeroelastic stability of suspension bridges using CFD

Stærdahl, J.W.; Sørensen, Niels N.; Nielsen, S.R.K.

Published in:
Shell and spatial structures: Structural architecture - towards the future looking to the past

Publication date:
2008

Aeroelastic Stability of Suspension Bridges using CFD

Jesper STÆRDAHL
Assistant professor
Aalborg University
Aalborg, Denmark

Niels SØRENSEN
Professor
Aalborg University
Aalborg, Denmark

Søren NIELSEN
Professor
Aalborg University
Aalborg, Denmark

Summary

In recent years large span suspension bridges with very thin and slender profiles have been built without proportional increasing torsional and bending stiffness. As a consequence large deformations at the mid-span can occur with risk of aeroelastic instability and structural failure. Analysis of aeroelastic stability also named flutter stability is mostly based on semi-empirical engineering models, where model specific parameters, the so-called flutter derivatives, need calibration from wind tunnel tests or numerical methods. Several papers have been written about calibration of flutter derivatives using CFD models and the aeroelastic stability boundary has been successfully determined when comparing two-dimensional flow situations using wind tunnel test data and CFD methods for the flow solution and two-degrees-of-freedom structural models in translation perpendicular to the flow direction and rotation around the span axis of the bridge section. These models assume that the main contributing modal modes of the bridge are the first bending mode and the first torsional mode. The present work focuses on numerical evaluation of the flutter instability using an arbitrary number of modes describing the structural deformation. Furthermore, flutter derivatives are evaluated by CFD models using forced motion of a bridge section in a two-dimensional virtual wind tunnel. The parameter region of critical values is shown to be outside measured values. It is shown that a rough extrapolation of the measured values may lead to erroneous results and CFD simulations may be used for extrapolation into the critical region. The flow analysis serves as preliminary studies for evaluating flutter stability using CFD methods in three dimensions, where the span-wise correlation of vortex separation, skew inflow, and effects from cables at the mid-span are to be considered.

Keywords: CFD; Suspension bridges; flutter derivatives; aeroelastic stability.

1. Introduction

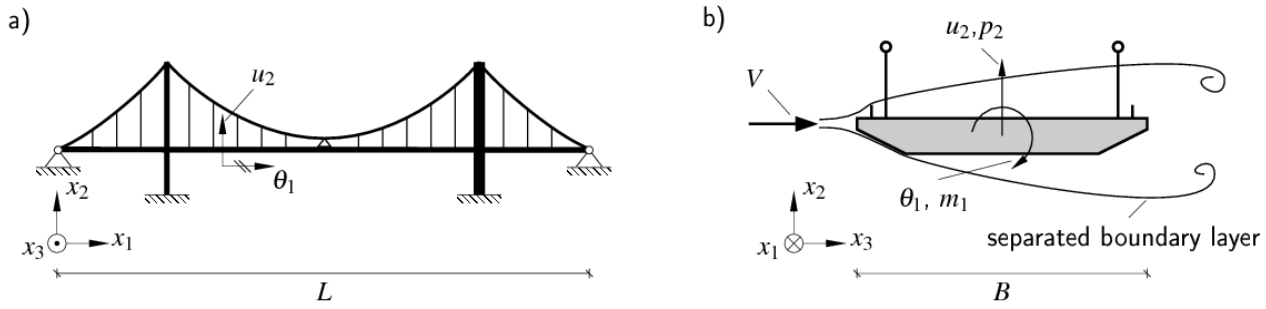

Fig. 1 Definition of notation. a) Principle structural setup of a suspension bridge. b) Cross section of bridge deck.

With ever increasing span lengths without proportional increase of the torsion and bending stiffness, modern suspension bridges become susceptible to aeroelastic instability and excessive vibrations when exposed to strong turbulent wind. Due to sharp edges and railings the boundary layer will generally be fully separated almost from the leading edge as illustrated in Fig. 1.

Aeroelastic stability analysis of suspension bridges is mostly based on engineering models defined by the pioneering work by Davenport [1] and later by Scanlan [2,3] using the so-called empirical determined flutter derivatives for aeroelastic loading on a reduced degree-of-freedom structural model. These represent a kind of frequency response functions for the aeroelastic loads due to forced harmonic motions of the bridge deck.

The underlying aerodynamic theory is basically two-dimensional, and presumes that parameters of the theory such as static force and moment coefficients, flutter derivatives and aerodynamic admittance functions are determined experimentally in model tests in a wind tunnel. The effect of along-wind response has been included in the 2D-approach,

>

at the expense of increasing the number of flutter derivatives from 12 to 18, [4]. When applied to time domain simulations, the flutter derivatives and aerodynamic admittance functions are typically approximated by low order rational functions for which the corresponding impulse response functions are directly available, making direct time integration possible at the expense of introducing additional filter state variable, Chen and Kareem [5,6]. The indicated filter variables account for various delay effects, e.g. the transient circulation built up following any instantaneous change of the effective angle of attack.

Attempts have been made to take the aerodynamic non-linearity into account by linearizing the loads around a static angle of torsion, [7,8,9]. This implies that the aerodynamic coupling constants (flutter derivatives and aerodynamic admittance functions), in addition to a dependence on frequency and Reynold's number, also become a function of the said angle. However, large suspension bridges are relatively flexible, and may undergo relatively large deformations. This questions the application of any linear load model, which in principle is based on the linearization of the loads around a given fixed position of the bridge.

3D-effects caused by oblique incoming wind have been taken into account in the same way by determining the flutter derivatives in the wind tunnel with the model section skewed to the along wind, [10]. The component of the skewed incoming wind along the bridge deck will convey a separated boundary layer pattern at a certain position to other positions on the bridge, and in this way introduce a certain delayed coherence of the flow pattern along the bridge. This convection is partly constrained by the sidewalls of the wind tunnel in the indicated model test. Neither has it been adequately considered elsewhere in the literature.

Still, another 3D-effect is the influence of the cables on the flow over the bridge deck at the mid-span. This may influence the modal loads of symmetric bending and torsion modes significantly, which have maximum amplitude at this position.

All the 3D-effects mentioned can be treated in wind tunnel tests of a full-model bridge. Since such tests have to be performed at scales as small as say 1:100, the tests suffer from inherent problems to reproduce the real flow pattern and dynamic behaviour of the bridge. Especially the along-span correlation of turbulence can be very difficult to simulate.

To improve the understanding of both 2D- and 3D-flows over the bridge sections and the coupled fluid structure problem, CFD (Computational Fluid Dynamics) is a possible supplement to the simpler aerodynamic models and wind tunnel tests typically used. In recent years, the progress in computer speeds, numerical methods and turbulence modelling have made it feasible to resolve the flow over bridge sections with a high degree of details. This has resulted in a series, of mainly 2D-studies of the fluid structure problem of the flow around 2D-bridge sections using CFD type codes; see [11,12,13,14,15,16].

The idea of the paper is to determine the flutter stability of the Great-Belt bridge using measured flutter derivatives from the literature and comparing these measurements with CFD simulations of the considered cross section. Often only the lowest plunge and pitch mode are used for evaluating the critical flutter velocity. In the present work an approach for determining the critical velocity using an arbitrary number of modes is devised. A numerical example where results from using the 8 lowest modes is presented. Finally, the numerical evaluated flutter derivatives are used for finding the flutter velocity. The results are compared with the case where flutter derivatives from measurements are used.

2. Theory

A global (x_1, x_2, x_3)-coordinate system is introduced as shown in Fig. 1a. Global displacement components $u_k(x_1, t)$ and rotation components $\theta_k(x_1, t)$ of a given section of the bridge deck defined by the x_1-coordinate are stored in the vector $u(x_1, t)$ defined as

$$u^T(x_1, t) = [u_1(x_1, t), u_2(x_1, t), u_3(x_1, t), \theta_1(x_1, t), \theta_2(x_1, t), \theta_3(x_1, t)] \quad (1)$$

Displacement and rotational components of the jth eigenmode of the bridge deck are stored in the vector

$$\Phi^{(j)\,T}(x_1) = [U_1^{(j)}(x_1), U_2^{(j)}(x_1), U_3^{(j)}(x_1), \Theta_1^{(j)}(x_1), \Theta_2^{(j)}(x_1), \Theta_3^{(j)}(x_1)] \quad (2)$$

Then, the displacement vector may be represented by the modal decomposition

$$u(x_1, t) = \sum_{j=1}^{\infty} \Phi^{(j)}(x_1) q_j(t) \quad (3)$$

< >

$q_j(t)$ represents the jth undamped modal coordinate. These are given by the following ordinary differential equation

$$M_j(\ddot{q}_j + 2\zeta_j\omega_j\dot{q}_j + \omega_j^2 q_j) = F_j(t) \quad , \quad j = 1,2,\ldots \tag{4}$$

where ω_j is the undamped circular eigenfrequency, ζ_j is the damping ration, M_j *i*s the modal mass, and $F_j(t)$ is the modal load in the jth mode. Because the structural damping of the bridge is low, and the important eigenfrequencies are well separated, modal decoupling via the structural damping has been assumed. Further, it should be noticed that the modal mass includes contributions both from the bridge deck and the pylons, cables and hangers. Only a load per unit length $p_2(x_1,t)$ in the x_2-direction and a torsional moment per unit length $m_1(x_1,t)$ in the x_1-direction are acting on the bridge deck. Then, the modal load becomes

$$F_j(t) = \int_0^L (U_2^{(j)}(x_1)p_2(x_1,t) + \Theta_1^{(j)}(x_1)m_1(x_1,t))dx_1 \tag{5}$$

where L is the entire length of the bridge deck. The said loads are assumed to be self-induced by the motion of the bridge deck. Further, a linearized 2D description of the basically non-linear flow is assumed. Then, the following expressions for the external loads on the bridge deck may be postulated

$$p_2(x_1,t) = \frac{1}{2}\rho V^2 B(KH_1^*(K)\frac{\dot{u}_2}{V} + KH_2^*(K)B\frac{\dot{\theta}_1}{V} + K^2H_3^*(K)\theta_1) \tag{6}$$

$$m_1(x_1,t) = \frac{1}{2}\rho V^2 B^2(KA_1^*(K)\frac{\dot{u}_2}{V} + KA_2^*(K)B\frac{\dot{\theta}_1}{V} + K^2A_3^*(K)\theta_1) \tag{7}$$

where ρ is the mass density of air, V is the wind velocity, and B is the width of the bridge deck. $H_1^*(K), H_2^*(K), H_3^*(K), A_1^*(K), A_2^*(K), A_3^*(K)$ are non-dimensional real functions, so-called flutter derivatives, depending on the reduced frequency K (and Reynold's number) defined as

$$K = \frac{B\omega}{V} \tag{8}$$

(6) and (7) only make sense for harmonically varying motions of the bridge deck at the circular frequency ω. Then, the flutter derivatives specify the frequency response functions for the indicated loads due to forced harmonically varying motions of the bridge deck. Due to the postulated 2D-character of the flow the flutter derivatives may be determined in 2D-wind tunnel tests.
The displacement components $u_2(x_1,t)$ and $\theta_1(x_1,t)$ may be represented by the following modal expansions

$$\left.\begin{aligned} u_2(x_1,t) &= \sum_{j=1}^{\infty} U_2^{(j)}(x_1)q_j(t) \\ \theta_1(x_1,t) &= \sum_{j=1}^{\infty} \Theta_1^{(j)}(x_1)q_j(t) \end{aligned}\right\} \tag{9}$$

The modal expansions for $u_2(x_1,t)$ and $\theta_1(x_1,t)$ as follow from (3) are inserted into (6) and (7), and the results are inserted into the modal loads (5), leading to

$$F_j(t) = \sum_{k=1}^{\infty} k_{jk}(\omega,V)q_k(t) + c_{jk}(\omega,V)\dot{q}_k(t) \tag{10}$$

$$\begin{aligned} k_{jk}(\omega,V) = {} & \frac{1}{2}\rho V^2 BK^2 H_3^* \int_0^L U_2^{(j)}(x_1)\Theta_1^{(k)}(x_1)dx_1 + \\ & \frac{1}{2}\rho V^2 B^2 K^2 A_3^* \int_0^L \Theta_1^{(j)}(x_1)\Theta_1^{(k)}(x_1)dx_1 \end{aligned} \tag{11}$$

$$\begin{aligned} c_{jk}(\omega,V) = {} & \frac{1}{2}\rho VBKH_1^* \int_0^L U_2^{(j)}(x_1)U_2^{(k)}(x_1)dx_1 + \frac{1}{2}\rho VB^2 KH_2^* \int_0^L U_2^{(j)}(x_1)\Theta_1^{(k)}(x_1)dx_1 + \\ & \frac{1}{2}\rho VB^2 KA_1^* \int_0^L \Theta_1^{(j)}(x_1)U_2^{(k)}(x_1)dx_1 + \frac{1}{2}\rho VB^3 KA_2^* \int_0^L \Theta_1^{(j)}(x_1)\Theta_1^{(k)}(x_1)dx_1 \end{aligned} \tag{12}$$

< >

Because of the symmetry of the bridge around the plane A shown in Fig. 3, the mode shape components $U_2^{(j)}(x_1)$ and $\Theta_1^{(j)}(x_1)$ will either be symmetric or skew-symmetric functions of x_1 around the said plane. Hence, integrals of symmetric and a skew-symmetric mode shape components in (11) and (12) will cancel. Further, $\Theta_1^{(j)}(x_1) \equiv 0$ in symmetric or skew-symmetric bending modes, and $U_2^{(j)}(x_1) \equiv 0$ in symmetric or skew-symmetric torsional modes. Hence, this cancels an additional number of the components $k_{jk}(\omega, V)$ and $c_{jk}(\omega, V)$. With the ordering of the eigenmodes as indicated in Table 1 the modal equations of motion may be recasted into the following matrix form

Table 1 Ordering and symmetry properties of modes

mode	$U_2^{(j)}(x_1)$	$\Theta_1^{(j)}(x_1)$
1	1st symmetric	0
2	0	1st symmetric
3	1st skew-symmetric	0
4	0	1st skew-symmetric
5	2nd symmetric	0
6	0	2nd symmetric
7	2nd skew-symmetric	0
8	0	2nd skew-symmetric

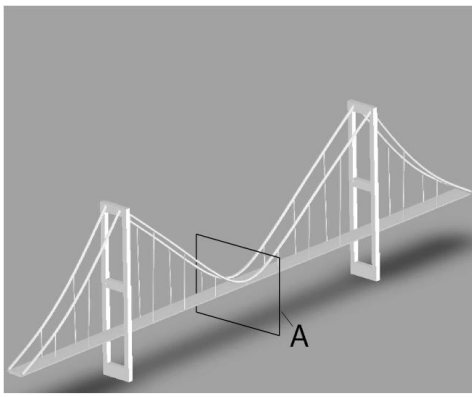

Fig. 2 Definition of symmetry planes.

$$\mathbf{m}\ddot{\mathbf{q}} + \mathbf{c}\dot{\mathbf{q}} + \mathbf{k}\mathbf{q} = \mathbf{c}_0(\omega, \mathrm{V})\dot{\mathbf{q}} + \mathbf{k}_0(\omega, \mathrm{V})\mathbf{q} \tag{13}$$

$$\mathbf{q}^{\mathrm{T}}(t) = [q_1(t), q_2(t), q_3(t), q_4(t), q_5(t), \cdots] \tag{14}$$

$$\mathbf{m} = \begin{bmatrix} M_1 & 0 & \cdots \\ 0 & M_2 & \cdots \\ \vdots & \ddots & \vdots \end{bmatrix}, \mathbf{c} = \begin{bmatrix} 2\zeta_1\omega_1 M_1 & 0 & \cdots \\ 0 & 2\zeta_2\omega_2 M_2 & \cdots \\ \vdots & \ddots & \vdots \end{bmatrix}, \mathbf{k} = \begin{bmatrix} \omega_1^2 M_1 & 0 & \cdots \\ 0 & \omega_2^2 M_2 & \cdots \\ \vdots & \ddots & \vdots \end{bmatrix} \tag{15}$$

$$\mathbf{k}_0(\omega, V) = \begin{bmatrix} 0 & k_{12} & 0 & 0 & 0 & k_{16} & 0 & 0 & 0 & k_{1\,10} & \cdots \\ 0 & k_{22} & 0 & 0 & 0 & k_{26} & 0 & 0 & 0 & k_{2\,10} & \cdots \\ 0 & 0 & 0 & k_{34} & 0 & 0 & 0 & k_{38} & 0 & 0 & \cdots \\ 0 & 0 & 0 & k_{44} & 0 & 0 & 0 & k_{48} & 0 & 0 & \cdots \\ 0 & k_{52} & 0 & 0 & 0 & k_{56} & 0 & 0 & 0 & k_{5\,10} & \cdots \\ 0 & k_{62} & 0 & 0 & 0 & k_{66} & 0 & 0 & 0 & k_{6\,10} & \cdots \\ 0 & 0 & 0 & k_{74} & 0 & 0 & 0 & k_{78} & 0 & 0 & \cdots \\ 0 & 0 & 0 & k_{84} & 0 & 0 & 0 & k_{88} & 0 & 0 & \cdots \\ \vdots & \vdots & \vdots & \vdots & \vdots & \vdots & \vdots & \vdots & \vdots & \vdots & \ddots \end{bmatrix} \tag{16}$$

$$\mathbf{c}_0(\omega, V) = \begin{bmatrix} c_{11} & c_{12} & 0 & 0 & c_{15} & c_{16} & 0 & 0 & c_{19} & c_{1\,10} & \cdots \\ c_{21} & c_{22} & 0 & 0 & c_{25} & c_{26} & 0 & 0 & c_{29} & c_{2\,10} & \cdots \\ 0 & 0 & c_{33} & c_{34} & 0 & 0 & c_{37} & c_{38} & 0 & 0 & \cdots \\ 0 & 0 & c_{43} & c_{44} & 0 & 0 & c_{47} & c_{48} & 0 & 0 & \cdots \\ c_{51} & c_{52} & 0 & 0 & c_{55} & c_{56} & 0 & 0 & c_{59} & c_{5\,10} & \cdots \\ c_{61} & c_{62} & 0 & 0 & c_{65} & c_{66} & 0 & 0 & c_{69} & c_{6\,10} & \cdots \\ 0 & 0 & c_{73} & c_{74} & 0 & 0 & c_{77} & c_{78} & 0 & 0 & \cdots \\ 0 & 0 & c_{83} & c_{84} & 0 & 0 & c_{87} & c_{88} & 0 & 0 & \cdots \\ \vdots & \vdots & \vdots & \vdots & \vdots & \vdots & \vdots & \vdots & \vdots & \vdots & \ddots \end{bmatrix} \tag{17}$$

< >

At application the modal expansion is truncated, and the system matrices $\mathbf{m}$, $\mathbf{c}$, $\mathbf{k}$, $\mathbf{k}_0(\omega, V)$ and $\mathbf{c}_0(\omega, V)$ become finite quadratic matrices. As seen from (15), (16) and (17) the modal coordinates $q_1(t)$, $q_2(t)$, $q_5(t)$, $q_6(t)$, $q_9(t)$, $q_{10}(t)$, ... are decoupled from the modal coordinates $q_3(t)$, $q_4(t)$, $q_7(t)$, $q_8(t)$, ... It turns out that instability only takes place among the former modal coordinates. Hence, the latter can be extracted from the equations of motion, reducing the dimension of stability analysis to half the magnitude. At small wind velocities the system is stable in the sense that a given perturbation from the equilibrium state $\mathbf{q}(t) = \dot{\mathbf{q}}(t) = \mathbf{0}$ is damped out in harmonic vibrations with an exponential decreasing amplitude. On the other hand at a very large wind velocity the harmonic vibrations becomes unstable with exponentially increasing amplitudes. Hence, a critical wind velocity V_c exists, where the structure performs harmonic vibrations with constant amplitudes. Then, at the critical wind velocity the solution has the form

$$\mathbf{q}(t) = \mathbf{q}_0 \mathrm{e}^{\mathrm{i}\omega t} \tag{18}$$

where ω is the so-called circular flutter frequency. Insertion of (18) into (13) provides the following non-linear eigenvalue problem for the determination of ω and V_c

$$(-\omega^2\mathbf{m} + \mathrm{i}\omega(\mathbf{c} - \mathbf{c}_0(\omega, V_c)) + (\mathbf{k} - \mathbf{k}_0(\omega, V_c)))\mathbf{q}_0 = \mathbf{0} \tag{19}$$

Non-trivial solutions $q_0 \neq 0$ only exists if the coefficient matrix is singular, leading to the flutter condition

$$\det(-\omega^2\mathbf{m} + \mathrm{i}\omega(\mathbf{c} - \mathbf{c}_0(\omega, V_c)) + (\mathbf{k} - \mathbf{k}_0(\omega, V_c))) = 0 \tag{20}$$

(20) must be fulfilled for the real and imaginary part of the determinant, which provides two non-linear equations for the determination of ω and V_c.

A numerical evaluation of the flutter derivatives using CFD methods assumes a harmonic variation of $u_2(t) = \tilde{u}_2 e^{i\omega t}$ and $\theta(t) = \tilde{\theta} e^{i\omega t}$, with the circular frequency ω and real amplitude $\tilde{u}_2$ and $\tilde{\theta}$. Inserting in (6) and (7) and assuming the lift and moment to vary harmonic with the same frequency and a phase ϕ relative to the motion, the following is obtained

$$\begin{aligned} \tilde{c}_L \mathrm{e}^{i(\omega t - \phi)} &= K^2(iH_1^*(K)\frac{\tilde{u}_2}{B} + (iH_2^*(K) + H_3^*(K))\tilde{\theta}_1)\mathrm{e}^{i\omega t} \\ \tilde{c}_M \mathrm{e}^{i(\omega t - \phi)} &= K^2(iA_1^*(K)\frac{\tilde{u}_2}{B} + (iA_2^*(K) + A_3^*(K))\tilde{\theta}_1)\mathrm{e}^{i\omega t}. \end{aligned} \tag{21}$$

where $p_2(t) = \frac{1}{2}\rho V^2 B \tilde{c}_L \mathrm{e}^{i(\omega t - \phi)}$ and $m_1(t) = \frac{1}{2}\rho V^2 B^2 \tilde{c}_M \mathrm{e}^{i(\omega t - \phi)}$ are given in terms of the non-dimensional lift and moment coefficients, respectively. A simulation with harmonic translation of the bridge deck and a simulation with harmonic rotation of the bridge deck as indicated above is made from which $\tilde{c}_L$, $\tilde{c}_M$ and ϕ can be identified from the numerical simulated lift and moment forces. This gives the following 6 conditions for determining the 6 flutter derivatives

$$\begin{aligned} &\mathrm{Im}(\frac{\tilde{c}_L B \mathrm{e}^{i\phi}}{K^2\tilde{u}_2}) = H_1^*, \quad \mathrm{Im}(\frac{\tilde{c}_L \mathrm{e}^{i\phi}}{K^2\tilde{\theta}_1}) = H_2^*, \quad \mathrm{Re}(\frac{\tilde{c}_L \mathrm{e}^{i\phi}}{K^2\tilde{\theta}_1}) = H_3^* \\ &\mathrm{Im}(\frac{\tilde{c}_M B \mathrm{e}^{i\phi}}{K^2\tilde{u}_2}) = A_1^*, \quad \mathrm{Im}(\frac{\tilde{c}_M \mathrm{e}^{i\phi}}{K^2\tilde{\theta}_1}) = A_2^*, \quad \mathrm{Re}(\frac{\tilde{c}_M \mathrm{e}^{i\phi}}{K^2\tilde{\theta}_1}) = A_3^*, \end{aligned} \tag{22}$$

where the first 2 for H_1^* and A_1^* are used in combination with the harmonic translation simulation and the remaining 4 are used in combination with the harmonic rotation simulation.

3. Numerical example

In the numerical example the Great Belt Link of Denmark is used with a mid-span of 1624m and outer span of 535m and pylons with a height of 250m. The bridge deck is steel and the pylons are made of concrete. A finite element model has been developed for extracting the lowest eigenmodes and frequencies for flutter analysis. Numerical two-dimensional aerodynamic analyses have been performed on a bridge deck section for identifying the flutter derivatives.

The aerodynamic simulations are performed with the incompressible Navier-Stokes solver EllipSys2D [19,20,21]. The code is second order accurate in time using the PISO algorithm of [18], and four sub-iterations per time step. The dimensionless time step used in the actual simulations is equal to $\Delta t^* = \frac{\Delta t V}{B} = 0.01$. In space the code is second order accurate, using central differences for the diffusive terms and the third order accurate QUICK scheme for the convective terms [23]. The turbulence in the boundary layer of the bridge is modelled by the k-ω SST model ,[24].
The computational grid is generated with the 2D hyperbolic grid generation program [22]. The grid topology is a so called O-configuration, and has 256 cells in the chordwise direction and 64 cells in the normal direction. Grid independence test was performed with half the number of cells in each direction. The grid around the profile is illustrated in Fig. 3a and the velocity vector field result from a steady simulation is visualized in Fig. 3b.

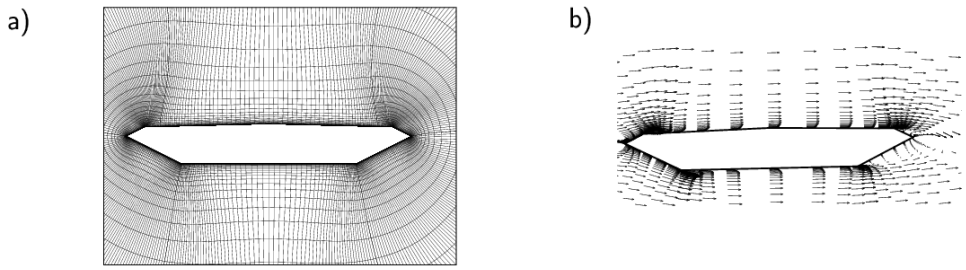

Fig. 3 a) Fine mesh around the bridge section. b) Velocity field visualization.

The lift and moment coefficients determined by numerical simulations are shown in Fig. 4 where (——) indicate results from a fine mesh simulation and (- - -) indicate results from a coarse mesh simulation. The illustrated results are for a pitch case with a periode of 54s. As seen, a significant harmonic component is present with a frequency equal the pitching frequency. Also a significant high frequency component is present on the fine mesh due to vortex shedding. In the present approach the high frequency component is filtered out from the flutter analysis. On the coarse grid the vortex shedding is not capture, but the deformation frequency component in the loads are present with the same frequency and phase as for the fine mesh results. However, an increase of the mean value of the lift is observed, but with no influence of the evaluated flutter derivatives. Hence, a coarse mesh can be used for evaluating flutter derivatives. Furthermore, numerical evaluated flutter derivatives where calculated for Reynold's number equal the one used for measurements without changes in the results.

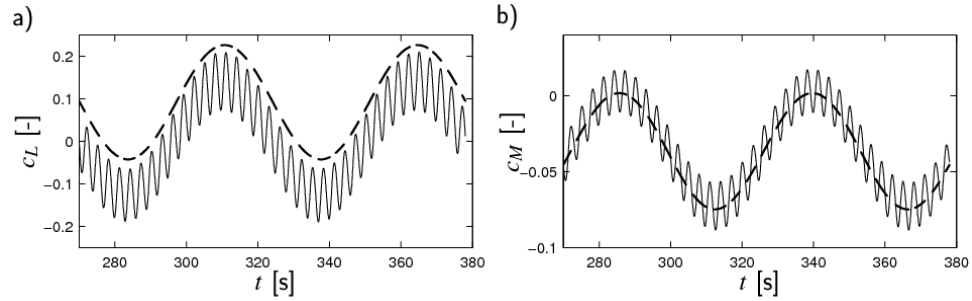

Fig. 4 Lift and moment coefficients determined by numerical simulations. Harmonic pitch with periode T=54s, $2\pi V/\omega B=9$. a) c_L (t). c_M (t). (——) Solution on fine mesh. (- - -) Solution on coarse mesh.

By a least-square-error method the amplitude and phase between the motion and forces are extracted from $c_L(t)$ and $c_M(t)$ and (22) is used to determine the flutter derivatives. In Fig. 5 the numerical evaluated flutter derivatives are compared with wind tunnel test data from Reinhold et al. [17]. Third degree polynomiums are fitted to the experimental data. As seen, the qualitative and quantitative variations are captured by the numerical analyses. However, at large values for $\frac{2\pi V}{\omega B}$ the numerical solution deviates from the extrapolations especially in A_2^* and H_2^* which are the terms on $\dot{\theta}$. It should be emphasized that extrapolations far from the measured data might be inaccurate, and also at low frequencies these terms might be hard to estimate accurately.

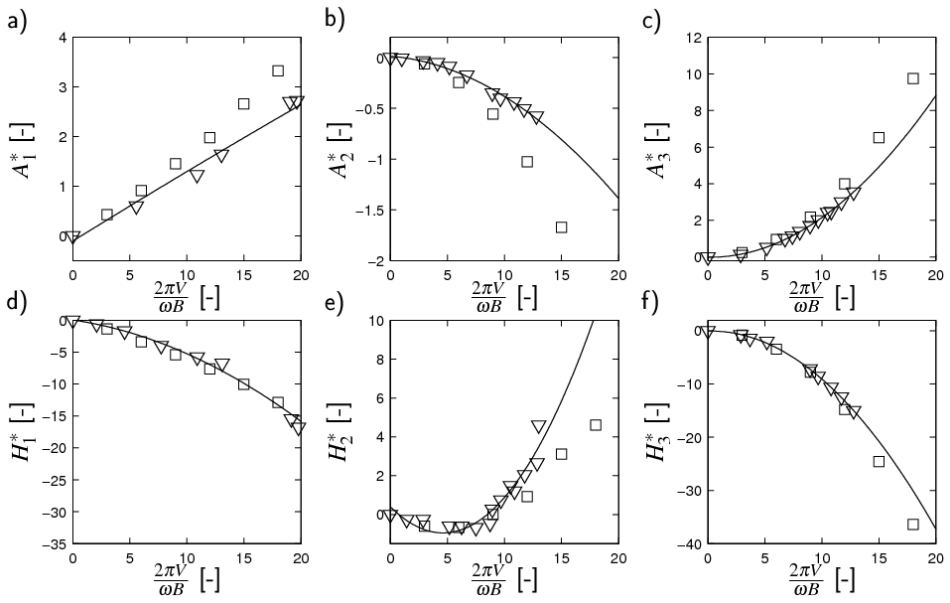

Fig. 3 Flutter derivatives. (∇) *Wind tunnel test results from Reinhold et al. [17].* (□) *CFD results.* (——) *Least square fit to Reinhold test data using 3rd degree polynomiums.*

Finally, the critical flutter velocity and frequency are determined using the modal approach described in the previous section. The determinant condition in (20) is evaluated for the decoupled problem using 2 or 8 modes. The results are shown in table 2.

Table 2 Critical values of from the flutter analysis.

modes	**flutter derivatives**	V_c	ω_c	$\frac{2\pi V_c}{\omega B}$
2	wind tunnel	100.9m/s	1.182 rad/s	17.3
8	wind tunnel	121.9m/s	1.101 rad/s	22.4
2	CFD	68.8m/s	1.152 rad/s	12.1
8	CFD	92.5m/s	1.095 rad/s	17.1

The flutter derivatives entering (20) are taken both as the wind tunnel test data (∇) and as the CFD results (□) from Fig. 5, respectively. By introducing higher modes a significant increase in the flutter velocity is obtained whereas the critical frequency is relatively constant. For the determined critical values the flutter derivatives are evaluated at a value larger than 15 where measurements are extrapolated and unreliable. When using the numerical evaluated flutter derivatives the velocity is significantly reduced but the same tendency as before is observed when introducing 8 modes instead of 2.

4. Conclusion

In the present work a two-dimensional flutter analysis is performed on the Great Belt Link suspension bridge. A method for introducing an arbitrary number of modes is devised. It is shown that the critical values of the flutter analysis are significantly changed when introducing more modes. The two-dimensional analysis is based on the method devised by Scanlan [2,3], where the so-called flutter derivatives enter. These coefficients are obtained from numerical CFD analysis and compared with wind tunnel measurements obtained from the litterature. It was shown that both qualitatively and quantitatively it is possible to obtain good results using CFD methods. However, the method devised by Scanlan does not include effects from vortex shedding, which introduce a significant high frequency component in the aerodynamic loads. Critical values for the flutter analysis are found in regions where it is necessary to perform extrapolation of measurements making these results uncertain. When the numerical evaluated flutter derivatives are used, a significant reduction of the flutter velocity is found. It can be concluded that the flutter analysis is relatively sensitive to the correct evaluation of flutter derivatives. A rough extrapolation may result in erroneous results. CFD results are easily obtained in

< >

the entire region and may be used for extrapolating measured flutter derivatives.

5. References

[1] DAVENPORT A.G., "Buffeting of a Suspension Bridge by Stormy Winds", *Journal of Structural Engineering*, ASCE, 88(3), 233-268, 1962.

[2] SCANLAN R.H., "The Action of Flexible Bridges under Wind, I: Flutter Theory" *Journal of Sound and Vibration*, 60(2), 187-199, 1978.

[3] SCANLAN R.H., "The Action of Flexible Bridges under Wind, II: Buffeting Theory", *Journal of Sound and Vibration*, 60(2), 201-211, 1978.

[4] KATSUCHI H. , JONES N.P., SCANLAN R.H. and AKIYAMA H., "Multi-mode Flutter and Buffeting Analysis of the Akashi-Kaikyo Bridge", *Journal of Wind Engineering and Industrial Aerodynamics*, 77 and 78, 431-441, 1998.

[5] CHEN X. and KAREEM A., "Advances in Modelling of Aerodynamic Forces on Bridge Decks", *Journal of Engineering Mechanics*, 128, 1193-1205, 2002.

[6] CHEN X. and KAREEM A., "New Frontiers in Aerodynamic Tailoring of Long Span Bridges: An Advanced Analysis Framework", *Journal of Wind Engineering and Industrial Aerodynamics*, 91, 1511-1528, 2003.

[7] SALVATORI L. and SPINELLI P., "Effects of Structural Nonlinearity and Along-Span Wind Coherence on Suspension Bridges: Some Simulation Results", *Journal of Wind Engineering and Industrial Aerodynamics*, 94, 415-430, 2006.

[8] X. ZHANG, H. XIANG and B. SUN, Nonlinear aerostatic and aerodynamic analysis of long-span suspension bridges considering wind-structure interactions. Journal of Wind Engineering and Industrial Aerodynamics, 90, 1065-1080, 2002.

[9] ZHU L.D. and XU Y.L. , "Buffeting Response of Long-Span Cable-Supported Bridges under Skew Winds. Part 1: Theory". *Journal of Sound and Vibration*, 281, 647-673, 2006.

[10] PANDEY M.D. and ARIARATNAM S.T., "Stability Analysis of Wind-Induced Torsional Motion of Slender Bridges", *Structural Safety*, 20, 379-389, 1998.

[11] SHIRAI S. and UEDA T., "Aerodynamic Simulation by CFD on Flat Box Girder of super-long-span Suspension Bridge", *Journal of Wind Engineering and Industrial Aerodynamics*, 91, 279-290, 2003.

[12] LARSEN A., WALTHER J.H., "Aeroelastic Analysis of Bridge Girder Sections Based on Discrete Vortex Simulations", *Journal Of Wind Engineering And Industrial Aerodynamics*, 67(8), 253-265,1997

[13] LARSEN A., WALTHER J.H., "Discrete Vortex Simulation of Flow Around Five Generic Bridge Deck Sections", *Journal Of Wind Engineering And Industrial Aerodynamics*, 77(8), 591-602, 1998.

[14] FRANDSEN J.B, "Numerical Bridge Deck Studies using Finite Elements. Part 1: Flutter", *Journal of Fluids and Structures*, 19(2), 171-191, 2004.

[15] WATANABE S., INOUE H. and FUMOTO K. "An Estimation of Static Aerodynamic Forces of Box Girders using Computational Fluid Dynamics", *Wind And Structures*, 7(1), 29-40, 2004.

[16] LIAW K.F., "Simulation of Flow around Bluff Bodies and Bridge Deck Sections using CFD." *Ph.D. thesis*. The University of Nottingham. June 2005.

[17] REINHOLD T.A., BRINCH M., DAMSGAARD Aa. "Wind tunnel test for the Great Belt Link", *Proc. 1st Int. Symposium on Aerodynamics of Large Bridges*, Rotterdam. 255-267, 1992

[18] ISSA R.I., "Solution of the Implicitly Discretised Fluid Flow Equations by Operator-Splitting", *J. Computational Phys.*, 62:40--65, 1985.

[19] MICHELSEN J.A., "Basis3D - a Platform for Development of Multiblock PDE Solvers", Technical Report AFM 92-05, Technical University of Denmark, 1992.

[20] MICHELSEN J.A., "Block structured Multigrid solution of 2D and 3D elliptic PDE's", Technical Report AFM 94-06, Technical University of Denmark, 1994.

[21] SØRENSEN N. N., "General Purpose Flow Solver Applied to Flow over Hills.", Risø-R- 827-(EN), Risø National Laboratory, Roskilde, Denmark, June 1995.

[22] SØRENSEN N.N. and HANSEN M.O.L. "Rotor Performance Predictions Using a Navier-Stokes Method.", *AIAA Paper* 98-0025, 1998.

[23] LEONARD B.P., "stable and accurate convective modelling procedure based on quadratic upstream interpolation", *Comput. Meths. Appl. Mech. Eng.*, 19:59--98, 1979.

[24] MENTER F. R. "Zonal Two Equation k-ω Turbulence Models for Aerodynamic Flows", *AIAA paper* 93-2906, 1993.